Intelligent Belt Drive Systems in Hybrid Powertrains: a Multipurpose Test Rig

Intelligent Belt Drive Systems in Hybrid Powertrains: a Multipurpose Test Rig

M. di Napoli * **M. Strähle** ** **S. Ruzimov** *
L. D. Suarez Cabrera * **N. Amati** * **A. Tonoli** *

* *Politecnico di Torino, Department of Mechanical and Aerospace Engineering, Mechatronics Laboratory, Corso Duca degli Abruzzi, 24, Torino, Italia (e-mail: maria.dinapoli@polito.it)*
** *Technische Universität Darmstadt, Karolinenplatz 5, 64289 Darmstadt, Deutschland*

Abstract: In traditional engine setups Belt Drive Systems (BDS) are in charge of power transmission from the crankshaft to the accessories. They are complex and critical dynamic mechanisms, involving contact mechanics and vibration phenomena. The hybridization of vehicles has increased the severity of the operating conditions of these systems that have become even more critical. The traditional alternator was substituted by a Belt-Starter Generator (BSG), an electric machine that can power the BDS in particular operating conditions to improve the Internal Combustion Engine (ICE) performance or to allow regenerative braking. The aim of the present work is to describe the design and the main characteristic of a test rig conceived to investigate in laboratory environment on the behaviour of belt drive systems in dynamic conditions. Two permanent magnet electric motors are used to replicate the dynamic behavior of crankshaft and BSG in a realistic, though controlled and repaetable, manner.

Keywords: Automotive Control, Hybrid Vehicles, Belt Drive Systems, Dynamic Modeling, Front-End Accessory Drives, Model Based Control

1. INTRODUCTION

Belt Drive Systems (BDS) or Front-End Accessory Drives (FEAD) constitute the traditional power transmission mechanism to power the main internal combustion ancilliaries such as the alternator, water pump and air conditioning pump. The torque generated by the Internal Combustion Engine (ICE) is transmitted by means of a serpentine belt that wraps around the driving and driven accessory pulleys of the drive systems.
BDS represent traditionally a complex and critical vehicle subsystem because of the performance specifications that need to be fulfilled. It usually in the severe ambient conditions of the engine compartment and is subject to highly dynamic excitations coming from the crankshaft harmonics. These harmonic excitation ,together with the inertia of the accessories (mainly the alternator), leads to vibrations of the belt and high tension fluctuations that can cause slippage and noise. To reduce these excitations a number of solutions have been developed including decoupling, filtering and overruning pulleys. The analysis of these phenomena led to the development of refined models of the belt pulley contact mechanics together with the definition of serpentine multi-pulley models to predict the dynamic response of serpentine belt-drive systems. A literature review shows that several research activities were carried out addressing separately the belt pulley mechanisms, see Bechtel et al. (2000), Rubin (2000), Hansson (1990), and the dynamic behavior of the transmission system, see Ulsoy et al. (1985), Hwang et al. (1994), Leamy and Perkins (1998). Only few attempts were done in the last 10 years to bridge the gap between research on contact mechanics and dynamic analysis by Leamy and Wasfy (2002), Leamy (2003), Kong and Parker (2003). Tonoli et al. (2006) analyzed the effect of shear deflection of the belt on the rotational dynamic behavior of the transmission.
Additionally, the advent of hybrid technologies has seen the rise of a class of micro-hybrids that changes the operating modes of the traditional belt drive systems. In this paradigm, the alternator is substituted with a Belt Starter Generator (BSG), an electrical machine able to work both as motor and as generator, causing a tight/slack span alternation when activated. The use of a BSG requires the introduction of a tensioning device able to keep the belt tension inside a safe range while preventing slippage facing the severe working conditions, see Cariccia et al. (2013). Several solutions have been proposed to satisfy this requirement, such as doble tensioners, decoupling tensioners and active electromechanical or hydraulica tensioners. With the addition of active devices, such as the BSG and complex tensioners, the intelligent BDS (iBDS) becomes a complex and challenging mechatronic system.
In this context, the present work aims to present a test rig that allows to study the BDS dynamics and power loss characteristics. Furthermore, the test rig offers major advantages over the utilization of traditional engine cells. Measurements obtained in such testing environments have a high level of uncertainty due to the uncontrollable irregularities that characterize the phiysical phenomena occuring into the ICE. The designed test rig allows the reproduction of a realistic and controllable testing environment. The use of two electric motors for the dynamic simulation of the

Table 1. Nomenclature

$AC =$	air conditioning
$AT =$	automatic tensioner
$b =$	belt
$bp =$	transition between belt and pulley
$BSG =$	belt-starter generator
$CS =$	crankshaft
$e_{BSG/CS} =$	error of belt-starter generator and crankshaft control
$F_{pAT} =$	force applied on automatic belt tensioner
$i_{dk} =$	direct current ($k = BSG, CS$)
$i_{qk} =$	quadrature current ($k = BSG, CS$)
$IDL =$	idler
$I_{BSG/CS} =$	current on belt-starter generator and crankshaft
$I_{CScont} =$	control current on crankshaft
$J_{pi}, C_{pi}, K_{pi} =$	rotational inertia, viscous damping and stiffness of i-th pulley($i = AC, BSG, CS, IDL$)
$J_{bi}, C_{bi}, K_{bi} =$	rotational inertia, viscous damping and stiffness of the arc of contact of i-th pulley ($i = AC, BSG, CS, IDL$)
$J_{pAT}, C_{pAT}, K_{pAT} =$	rotational inertia, viscous damping and stiffness of the automatic tensioner pulley
$K_{ek} =$	electromagnetic motor constant ($k = BSG, CS$)
$L_{dk} =$	direct inductance ($k = BSG, CS$)
$L_{qk} =$	quadrature inductance ($k = BSG, CS$)
$m_{aAT}, C_{aAT}, K_{aAT} =$	mass, viscous damping and stiffness of the arm of the automatic tensioner
$M_k =$	torque applied by the motor on the k-th shaft ($k = BSG, CS$)
$M_{pi} =$	torque applied by the belt on i-th pulley($i = AC, BSG, CS, IDL$)
$M_{CS} =$	output torque from crankshaft motor
$M_{BSGact/cont/ref} =$	actual, control and reference torque on belt-starter generator
$M_{CSact/cont/ref} =$	actual, control and reference torque on crankshaft
$p =$	pulley
$p_k =$	number of pole pairs ($k = BSG, CS$)
$R_k =$	coil resistance ($k = BSG, CS$)
$R_{pAT} =$	wrap radius on automatic belt tensioner pulley
$R_{pi} =$	wrap radius on i-th pulley ($i = AC, BSG, CS, IDL$)
$T =$	belt tension
$V_{dk} =$	direct voltage ($k = BSG, CS$)
$V_{qk} =$	quadrature voltage ($k = BSG, CS$)
$\alpha_{AT} =$	wrap angle of the automatic tensioner pulley
$\theta =$	angular displacement of the pulley
$\theta_{BSGact/cont/ref} =$	actual, control and reference angular of displacement of belt-starter generator
$\omega_{BSGact/cont/ref} =$	actual, control and reference angular velocity of belt-starter generator
$\omega_{CSact/cont/ref} =$	actual, control and reference angular velocity of crankshaft pulley
$\omega_{pAC/AT/BSG/CS/IDL} =$	angular velocity of the air conditioning, automatic tensioner, belt-starter generator, crankshaft and idler pulley
$\omega_{BSG/CS} =$	angular velocity of belt-starter generator and crankshaft

BSG and the crankshaft of the ICE allows to reproduce the different operating conditions of the iBDS. In addition, it is fundamental for taking into account the crankshaft oscillations due to the overlapping of the harmonics. The harmonics are generated via the Electronic Control Unit (ECU) in a predictable and repeatable manner.
The aim of this work is to describe the design and the obtained characteristics of the belt transmission test rig, highlighting its versatility. At first the main components of the test rig are described and complete details regarding the control and monitoring system are provided. Secondly the model of the system, divided into its main components, is presented and used for the definition of the specifications of the two electric motors.

2. EXPERIMENTAL SETUP AND TEST RIG CHARACTERISTICS

The design was performed to obtain the maximum versatility and allow the test rig reproducing different kind of BDS, both for what the mounting solutions and the characteristic of the components are concerned. The aim of the present section is to give an overview of the test rig and illustrate its main characteristics.

2.1 Mechanical layout

Fig. 1 shows the geometric configuration of the test rig from the top view. The layout reproduces the setup of a real engine front end, where the BDS connects five components: crankshaft, BSG, air conditioning compressor, automatic tensioner, idler pulley. The power is transmitted by a V-ribbed belt with 5 ribs. The layout was reproduced in a horizontal plane to have a uniform distribution of the forces acting on the frame and to avoid possible bending stresses on the bearing structure. The mounting solutions of the pulleys were adopted to allow the substitution of each pulley with others of different radii or coupled with belts of different number of ribs or type. The crankshaft (1) and BSG (3) pulleys were mounted on the shafts of two BoschRexroth IndraDyn H electric motors. The crankshaft is powered with motor MSS182D-0260 and the BSG with MSS102D-0800. Their specifications are listed in table 2. The frameless configuration of the two motors and their liquid cooling allowed to design their case to obtain the best integration with the rest of the test rig. On the shaft of the two motors were mounted two equal modular magnetic encoders ERM 2984 by Heidenhain (line count 192, $1V_{pp}$ sinusoidal incremental signals, maximum rotational speed $47000rpm$, power supply $5V_{dc}$). The angular speeds of the crankshaft and BSG pulleys are additionally monitored by means of two optical tacho sensors. These devices employ

Table 2. Characteristics of Electric Motors

Function	Rated Speed	Max Speed	Rated Torque	Max Torque	Rated Power	Rated Current	Max Current
	n $[rpm]$	n_{max} $[rpm]$	M $[Nm]$	M_{max} $[Nm]$	P $[kW]$	I $[A]$	I $[A]$
Crankshaft	2600	12000	140	320	38.1	71	200
BSG	8000	22500	20	45	16.8	24	69

Table 3. Parameters of Accessories

Position	Accessory	Pulley Diameter $[m]$	Coordinates [X,Y] $[m]$	Rotational Inertia $[kgm^2]$
1	Crankshaft	126.0 e-3	[0;0] e-3	53.4 e-3
2	Idler	65.0 e-3	[136.2;216.0] e-3	24.6 e-6
3	Alternator	54.0 e-3	[220.4;269.0] e-3	4.5 e-3
4	Air Conditioning	109.2 e-3	[177.1;97.0] e-3	2.2 e-3
5	Automatic Tensioner	65.0 e-3	[76.3;64.8] e-3	24.6 e-6

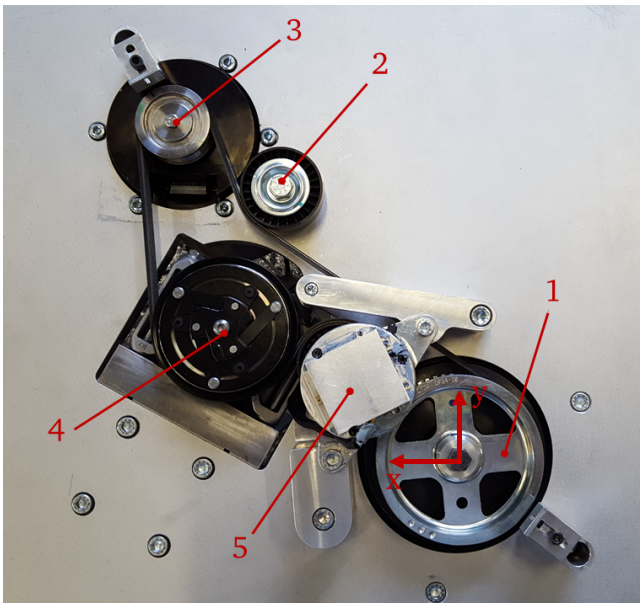

Fig. 1. Belt Drive Layout. The system is composed by: (1) crankshaft, (2) idler pulley, (3) BSG, (4) AC compressor, (5) automatic tensioner

a photoelectric sensor (OPB705 by Optek, power supply $5V_{dc}$) that detects the reflection of a line pattern printed onto the pulley surface. In order to measure the tension of the belt both in static and dynamic conditions the idler pulley (2) hub was instrumented with a load cell (DB-DA-750-17 by Magtrol, nominal force $750N$, power supply $5V_{dc}$). The AC compressor (4) was mounted as a unit to have the possibility to use it as a load, even though during the first experimental phase it will not be actuated and will behave just as an additional idler pulley. The automatic tensioner (5) installed on the test rig is a prototype that is able to adjust the belt tension in response to a software request input. The angular displacement of the tensioners pivot is measured by means of a magnetic angle sensor module (KMA210 by NXP, angle resolution $0.04deg$, maximum angle $180deg$, external magnetic field strength $35kA/m$, power supply $5V_{dc}$).
Table 3 provides data on geometric and inertial characteristics of the components of the test rig.

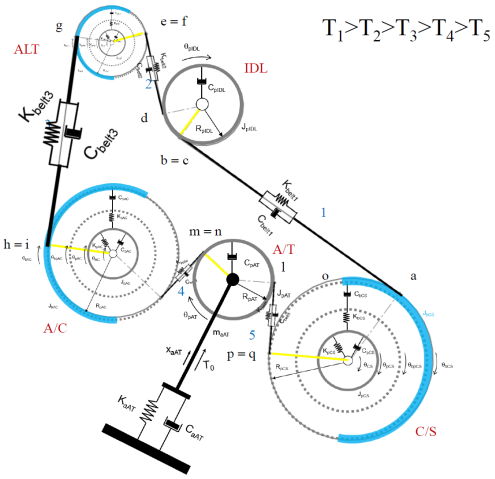

Fig. 2. Belt Drive lumped-parameter model

2.2 Control system

The control architecture of the test rig is composed by a high voltage control section for the two electric motors and a low voltage ECU that computes the reference speed to give as an input to the control loops of the two electric motors and of acquiring and analyzing the data read by the sensors mounted on the test rig. The power supply (HMV01.1R-W0065-A-07 by BoschRexroth) powers both the inverters that are connected onto the same DC BUS. The main feature of such supply unit is the possibility of power regeneration at the mains, meaning that the power produced by one of the two motors acting as alternator is given back to the network. The modular power section is completed by two BoschRexroth inverters, HMS01.1N-W0210 for Motor 1 and HMS01.1N-W0070 for Motor 2. The control sections (CSH01.1C-CO-ENS-EN2-MEM-L2-S) are the same for both inverters and provide three nested control loops: current, speed and position control. In the studied application the position control is not of interest, so such loop is not considered in the following analysis. The two inverters give the possibility of closing the control loops inside their firmwares but also outside by means of a dedicated control unit. The control laws implemented onto

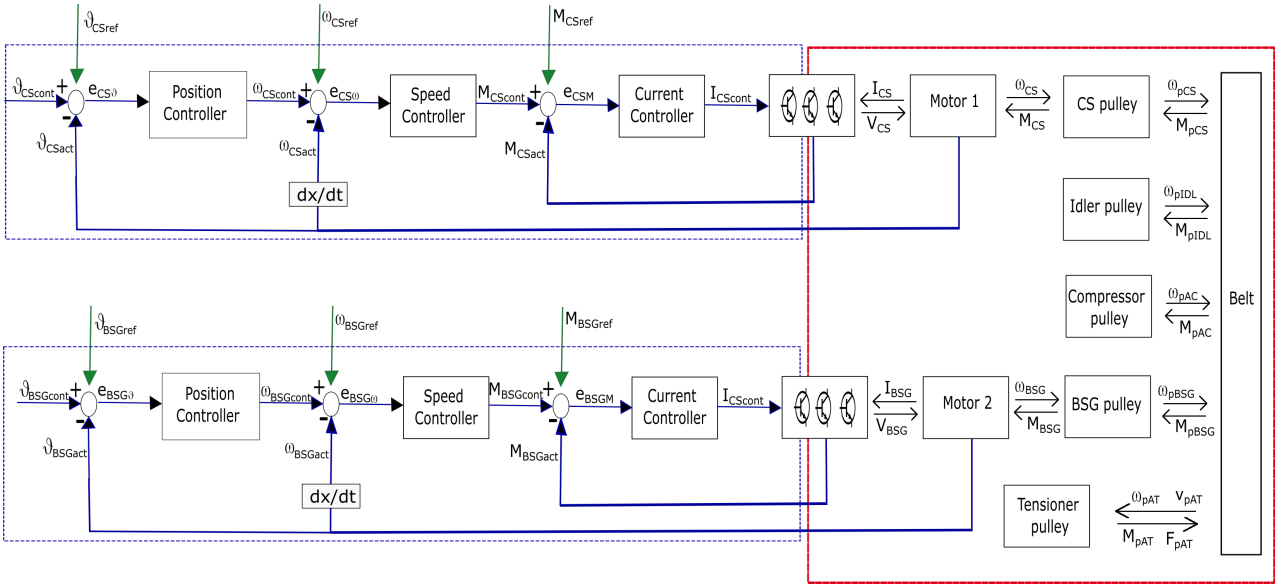

Fig. 3. Power and information exchanges of the system. In blue the information exchanges area, in red the bond-graph representation of the power transmission area

the inverters' firmware consisit of a Proportional-Integral (PI) compensator for each control loop. In Fig. 3 there are indicated the possible inputs that can be provided to the two inverters through the master communication and CANOpen Protocol. The two control sections allow the utilization of some optional features for analog and digital inputs and outputs, encoders acquisition, serial interface towards commissioning tool on PC, emulation of encoder data towards ECU, master communication with ECU through CANOpen Protocol.
The ECU is built around a Control Card based on a Texas Instruments floating point Digital Signal Processor (DSP). The Control Card is equipped with 16 ADC channels, capture and quadrature encoder modules and an asynchronous RAM which allows the real time acquisitions of the variables measured on the test rig by the sensors described above. Besides, the communication peripherals allow the use of the CANOpen protocol for communication towards the two inverters. The ECU is used to control the operations of the two motors, actuating the automatic belt tensioner and monitoring the parameters measured on the system.

3. SYSTEM MODEL AND SPECIFICATIONS DEFINITION

As shown in Fig. 3, the system is composed by two main subsystems: one characterized by a power exchange, including the electromechanical system comprising the power transmission and the two electric motors, the other by an information exchange, including the control architecture. The system operates in two main conditions: crankshaft driving the transmission, and BSG driving the transmission.
In the design phase of the test rig, the performance specifications were defined by means of a model of the BDS in the MATLAB-Simulink® environment. Such model is accurateliy described in Tonoli et al. (2006).
The present section briefly describes the modeling approach and its use for the design od the test bench.

3.1 Dynamic Model

The overall power transmission structure can be divided into 8 main components as shown in Fig. 3: belt, electric motors pulleys, A/C compressor, idler pulley, automatic tensioner pulley and electric motors. These subsystems are included in the red perimeter of Fig. 3, their interaction is described with the corresponding power variables. The causal form (input/output relations in each subsys-

Table 4. Equations of Power Transmission

Dynamic Behavior of Pulleys
$J_{bi}\ddot{\theta}_{bi} + K_{bi}(\theta_{bi} - \theta_{bpi}) = \Delta T R_{pi}$
$J_{pi}\ddot{\theta}_{pi} + K_{pi}(\theta_{pi} - \theta_i) - C_{bi}(\dot{\theta}_{bpi} - \dot{\theta}_{pi}) + C_{pi}(\dot{\theta}_{pi} - \dot{\theta}_i) = 0$
$K_{bi}(\theta_{bpi} - \theta_{pi}) + C_{bi}(\dot{\theta}_{bpi} - \dot{\theta}_{pi}) = 0$
Dynamic Behavior of Belt
Arcs of Contact on Pulley:
$M_{pi} = \Delta T R_{pi}$
Belt Spans:
$\Delta T = K_{bj}\Delta x + C_{bj}\Delta\dot{x}$
Dynamic Behavior of Automatic Tensioner
Rotational Behavior:
$J_{pAT}\ddot{\theta}_{pAT} + C_{pAT}\dot{\theta}_{pAT} = (T_3 - T_2)R_{pAT}$
Translational Behavior:
$m_{aAT}\ddot{x}_{AT} + C_{aAT}\dot{x}_{AT} + K_{aAT}x_{AT} = (T_3 + T_2)\sin(\frac{\alpha_{AT}}{2}) - T_0$
Dynamic Behavior of Electric Motors
Voltage generation:
$V_{qk} = R_k i_{qk} + L_{qk}\dot{i}_{qk} + k_e\dot{\theta}_k - L_{dk}p_k\dot{\theta}_k i_{dk}$
$V_{dk} = R_k i_{dk} + L_{qk}\dot{i}_{dk} + L_{qk}p_k\dot{\theta}_k i_{qk}$
Torque generation:
$M_k = K_{ek}\frac{3}{2}i_{qk}$

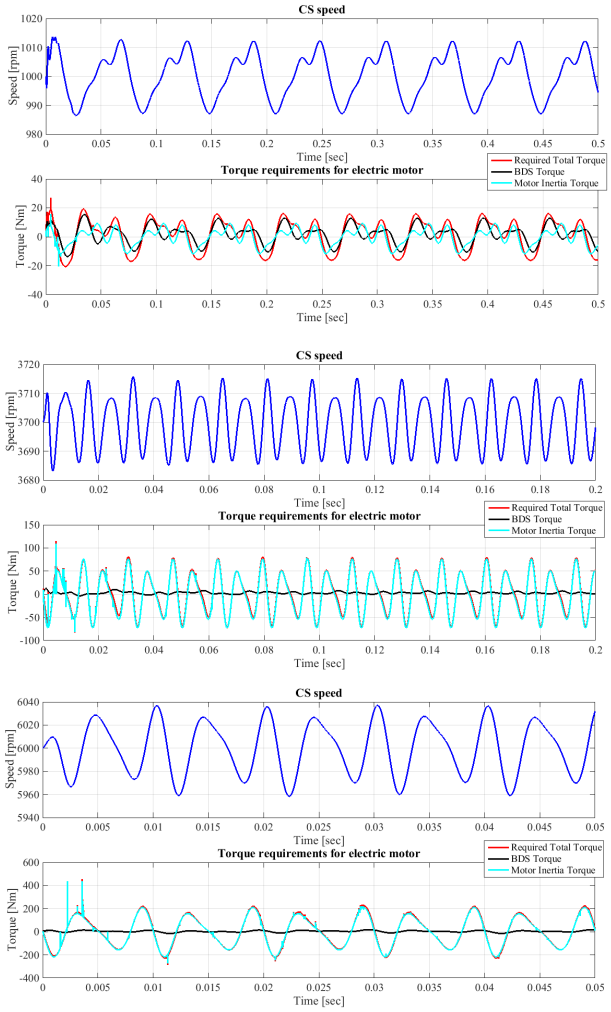

Fig. 4. Analysis of torque requirements for CS electric motor: in black, torque needed for operating the BDS; in light blue, torque needed to overcome the electric motor inertia; in red, resulting torque.

tem) shown in Fig. 3 corresponds to the case when the crankshaft powers the BDS. In such situation the BSG can act only as an alternator and generates a torque according to its speed. The role of the two motors can be exchanged, for example, when simulating an engine start-stop function.
From the electrical point of view, the voltage imposed to the CS electric motor by the corresponding inverter is the input to the system.
The modeling of each subsystem of the BDS was kept as simple as possible by using lumped parameters of inertia, stiffness and damping. The model described in Tonoli et al. (2006) was extended to a 5 pulleys configuration obtaining the lumped-parameter model of Fig. 2 that will be used to describe the system's dynamics and to define the performance specifications of the test rig.
Table 4 provides the equations that describe the dynamic behavior of each subsystem. The two electric motors were modeled using a dq-axis representation, including the effects of resistance, inductances and electromotive force.

3.2 ICE behavior reproduction

The performances of the motor are given by rated and maximum values of speed and torque and by the bandwidths reachable with current and velocity control loops. Consequently it was important to define such specifications, taking into account the desired reference values and dynamics, the layout characteristics and the additional inertia of the electric motor.
The definition of the required specifications took the following steps. Firstly, the required speed was derived by the operating speed values of the real ICE, which arrives to 6000 rpm. Secondly, the crankshaft speed imposed by the ICE to the crankshaft pulley was measured on an engine test cell. Amplitude and phase of the main harmonics were identified analitically by implementing a curve fitting procedure, using the formula in (1) as suggested by Genta and Morello (2009).

$$\omega_i = \omega_{mean} + \sum_{n=1}^{4} nA_n cos(\omega_{mean} t + \phi_n) \qquad (1)$$

As a first result, this identification process indicated the required bandwidth needed for speed and current control loops when running at different reference speed values.
Then, the identified speeds were given as a reference to the speed loop of the simulator that allowed the computation of the torque that the CS electric motor needs to provide. The analysis was performed for different electric motors available on the market, including their inertia values into the simulator. In Fig. 4 is shown the analysis of torque requirements at different speeds for the selected motor which has a low inertia value. In black is indicated the torque component needed for operating the BDS, in light blue the torque needed to overcome the electric motor inertia and in red the resulting torque that the motor will need to finally provide. As clearly highlighted by Fig. 4, the main contribution to the overall torque is required to overcome the electric motor inertia. This consideration allows to study the torque requirements taking into account only such contribution and motivated a design of the shafts with minimum inertia properties.
The selected electric motor by BoschRexroth represented the best trade-off between speed, bandwidth and torque requirements. Its rated and maximum speed are respectively $2600rpm$ and $12000rpm$, being therefore able to reach the desired $6000rpm$. The bandwidth of the current loop is equal to $520Hz$ if its PI controller is calibrated as indicated by the producer's specification for optimized performances. This leads to a maximum reachable bandwidth for the speed control loop of $260Hz$. Consequently, the motor allows to reproduce all the harmonic components with their amplitude values up to $4000rpm$, after this value 1^{st} and 2^{nd} harmonics will still be completely reproduced while 3^{rd} and 4^{th} will be attenuated but not eliminated provided we do not overcome the peak torque. The rated and maximum torque values are respectively $140Nm$ and $320Nm$. As shown in Fig.4 to a speed of $6000rpm$ corresponds a maximum torque of around $200Nm$ which can be fully reproduced with a duty cycle of 10% on a period of 10 minutes, which is sufficient for the tests that will be performed. The values of rated and maximum torque define the maximum amplitudes that the electric motor

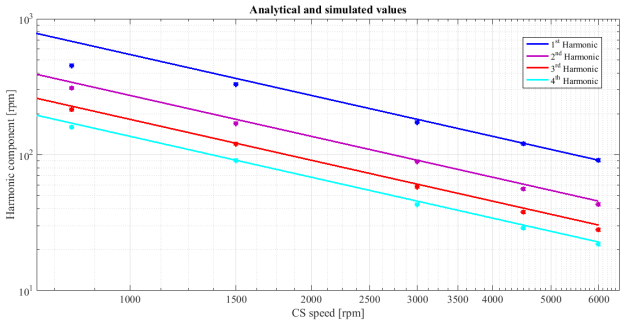

Fig. 5. Envelopes of harmonic contributions and comparison with simulation results

is capable of replicating for each harmonic. Such analysis was analytically performed taking into account only the electric motor inertia and then compared to the results of the simulations that included the BDS effects. Each harmonic component was considered autonomously and its contribution was caluclated and simulated neglecting the other components. The analytical calculations provided therefore the envelopes of the allowed amplitude values that are shown in Fig. 5. In Fig. 5 is also shown the comparison between calculated and simulated values. It is clear how the torque required for operating the BDS represents a small portion of the overall required torque. It is important to notice that at low speeds the torque required for the accessories, and in particular the alternator, become higher and no longer neglegible. This effect is particularly clear for what concerns the first harmonic.

3.3 BSG specifications

The definition of the BSG performances does not include an harmonic analysis but is detemined by the sole reachable speed and torque values. The reachable speed is obtained through the transmission ratio between BSG and CS pulleys of the BDS and the maximum speed requested for the CS motor. In this case to 6000rpm of the CS speed correspond 14000rpm of the BSG. The torque that the BSG needs to provide is given by the performances required for the different operating modes that define the BSG functionalities. Said operating modes can be divided into the following groups:

- Standard engine driving mode with BSG working as traditional alternator
- Regenerative braking
- Electric traction mode
- Warm engine start, i.e. warm cranking
- Cold engine start, i.e. cold cranking
- Electric boost, i.e. traction with ICE on

The maximum torque value was obtained in the cold cranking operating mode and it is equal to around 40Nm. In Fig.6 can be seen the torque-speed characteristic required for the BSG motor. Such requirement is completely fullfilled by the characteristics of the selected electric motor.

4. CONCLUSION

In the present work a test rig for the characterization of Belt Drive Systems was developed. The design focused on

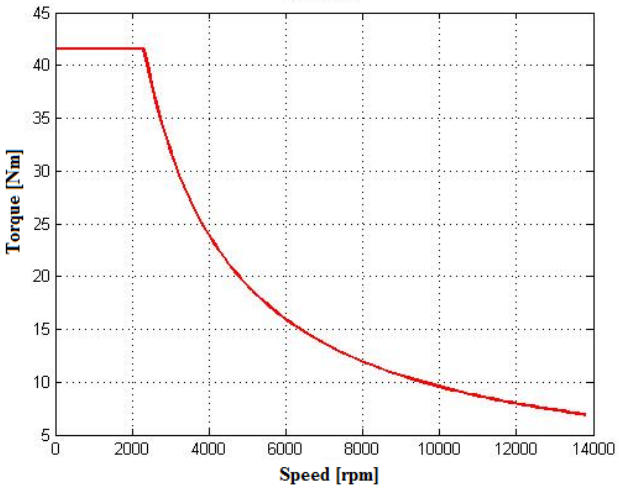

Fig. 6. Required BSG characteristic

the versatility of the test rig that is able to reproduce several kinds of transmissions, with different characteristics in terms of dimensions and performances. The actuation performed by means of two electric motors will allow the design of optimized control strategies for the reproduction of the realistic operating conditions of the mechanism. The test rig represents an advantageous tool for the analysis of the overall system if compared to a traditional engine cell. Not only the operating conditions are repeatabe but also the costs of the experimental tests are reduced.
The test rig is currently going through set up work and functional analysis in preparation for the experimental activities. The experiments will contemplate tests at constant speed imposed by the CS with varying torque requests from the BSG aimed at the complete validation of the model, the characterization of the slip phenomena at the contact surfaces of the pulleys and the power dissipation evaluation. Additional tests in dynamic conditions will be performed, simulating real operating conditions of crankshaft and BSG, for the evaluation of the natural frequencies of the transmission.

REFERENCES

Bechtel, S., Vohra, S., Jacob, K., and Carlson, C. (2000). The stretching and slipping of belts and fibers on pulleys. *Journal of Applied mechanics*, 67(1), 197–206.

Cariccia, G., Licata, F., and NOE, E. (2013). Actuated tensioner for an accessory drive. WO Patent App. PCT/IB2013/055,123.

Genta, G. and Morello, L. (2009). The automotive chassis: Volume 2: System design (mechanical engineering series).

Hansson, H. (1990). Geometry conditions for good power capacity in a v-ribbed belt drive. *Journal of Mechanical Design*, 112(3), 437–441.

Hwang, S.J., Perkins, N., Ulsoy, A., and Meckstroth, R. (1994). Rotational response and slip prediction of serpentine belt drive systems. *Journal of Vibration and Acoustics*, 116(1), 71–78.

Kong, L. and Parker, R.G. (2003). Equilibrium and belt-pulley vibration coupling in serpentine belt drives. *Journal of Applied Mechanics*, 70(5), 739–750.

Leamy, M. (2003). Dynamics analysis of the time-varying operation of belt-drives. In *ASME 2003 International Design Engineering Technical Conferences and Computers and Information in Engineering Conference*, 399–408. American Society of Mechanical Engineers.

Leamy, M.J. and Wasfy, T.M. (2002). Transient and steady-state dynamic finite element modeling of belt-drives. *Journal of Dynamic Systems, Measurement, and Control*, 124(4), 575–581.

Leamy, M. and Perkins, N. (1998). Nonlinear periodic response of engine accessory drives with dry friction tensioners. *Journal of Vibration and Acoustics*, 120(4), 909–916.

Rubin, M. (2000). An exact solution for steady motion of an extensible belt in multipulley belt drive systems. *Journal of Mechanical Design*, 122(3), 311–316.

Tonoli, A., Amati, N., and Zenerino, E. (2006). Dynamic modeling of belt drive systems: effects of the shear deformations. *Journal of vibration and acoustics*, 128(5), 555–567.

Ulsoy, A., Whitesell, J., and Hooven, M. (1985). Design of belt-tensioner systems for dynamic stability. *Journal of vibration, acoustics, stress, and reliability in design*, 107(3), 282–290.